Atmos. Chem. Phys. Discuss., https://doi.org/10.5194/acp-2019-121
Manuscript under review for journal Atmos. Chem. Phys.
Discussion started: 19 March 2019

Atmospheric Chemistry and Physics Discussions

Increased water vapour lifetime due to global warming

Øivind Hodnebrog[1], Gunnar Myhre[1], Bjørn H. Samset[1], Kari Alterskjær[1], Timothy Andrews[2], Oliviér Boucher[3,4], Gregory Faluvegi[5,6], Dagmar Fläschner[7], Piers M. Forster[8], Matthew Kasoar[9,10], Alf Kirkevåg[11], Jean-Francois Lamarque[12], Dirk Olivié[11], Thomas B. Richardson[8], Dilshad Shawki[9], Drew Shindell[13], Keith P. Shine[14], Philip Stier[15], Toshihiko Takemura[16], Apostolos Voulgarakis[9], and Duncan Watson-Parris[15]

[1]CICERO Center for International Climate Research, Oslo, Norway.
[2]Met Office Hadley Centre, Exeter, UK.
[3]Institut Pierre-Simon Laplace, Paris, France.
[4]CNRS / Sorbonne Université, Paris, France.
[5]NASA Goddard Institute for Space Studies, New York, USA.
[6]Center for Climate Systems Research, Columbia University, New York, USA.
[7]Max-Planck-Institut für Meteorologie, Hamburg, Germany.
[8]University of Leeds, Leeds, United Kingdom.
[9]Department of Physics, Imperial College London, London, UK.
[10]Grantham Institute – Climate Change and the Environment, Imperial College London, London, UK.
[11]Norwegian Meteorological Institute, Oslo, Norway.
[12]NCAR/UCAR, Boulder, USA.
[13]Duke University, Durham, USA.
[14]University of Reading, Reading, UK.
[15]Department of Physics, University of Oxford, UK.
[16]Kyushu University, Fukuoka, Japan.

Correspondence to: Øivind Hodnebrog (oivind.hodnebrog@cicero.oslo.no)

Abstract. The relationship between changes in integrated water vapour (IWV) and precipitation can be characterized by quantifying changes in atmospheric water vapour lifetime. Precipitation isotope ratios correlate with this lifetime, a relationship that helps understand dynamical processes and may lead to improved climate projections. We investigate how water vapour and its lifetime respond to different drivers of climate change, such as greenhouse gases and aerosols. Results from 11 global climate models have been used, based on simulations where CO_2, methane, solar irradiance, black carbon (BC), and sulphate have been perturbed separately. A lifetime increase from 8 to 10 days is projected between 1986-2005 and 2081-2100, under a business-as-usual pathway. By disentangling contributions from individual climate drivers, we present a physical understanding of how global warming slows down the hydrological cycle, due to longer lifetime, but still amplifies the cycle due to stronger precipitation/evaporation fluxes. The feedback response of IWV to surface temperature change differs somewhat between drivers. Fast responses amplify these differences and lead to net changes in IWV per degree surface warming ranging from 6.4±0.9%/K for sulphate to 9.8±2%/K for BC. While BC is the driver with the strongest increase in IWV per degree surface warming, it is also the only driver with a reduction in precipitation per degree surface warming. Consequently, increases in BC aerosol concentrations yield the strongest slowdown of the hydrological

Atmos. Chem. Phys. Discuss., https://doi.org/10.5194/acp-2019-121
Manuscript under review for journal Atmos. Chem. Phys.
Discussion started: 19 March 2019

cycle among the climate drivers studied, with a change in water vapour lifetime per degree surface warming of 1.1±0.4 days/K, compared to less than 0.5 days/K for the other climate drivers (CO_2, methane, solar irradiance, sulphate).

1 Introduction

Water vapour is the largest contributor to the natural greenhouse effect and the source of a major climate feedback mechanism (Boucher et al., 2013). Changes in the hydrological cycle will have widespread consequences for humanity, e.g., through changing precipitation patterns and extremes. The global-mean integrated water vapour (IWV) is found to increase by around 7%/K both in models (Held and Soden, 2006; O'Gorman and Muller, 2010) and observations (Wentz et al., 2007; O'Gorman et al., 2012), consistent with the rate of change of saturation vapour pressure with temperatures representative of the lower troposphere and constant relative humidity (Allen and Ingram, 2002; Trenberth et al., 2003; Held and Soden, 2006). Hence, recent observed moistening trends have been attributed to human activities (Santer et al., 2007; Chung et al., 2014).

In contrast to the expected increase in IWV, models project that global-mean precipitation will only rise by 1-3% per degree of surface warming, due to energetic constraints (Allen and Ingram, 2002; Held and Soden, 2006; O'Gorman et al., 2012). Extreme precipitation events, however, are likely to increase with the availability of water vapour (Allen and Ingram, 2002) (at around 7%/K), but large uncertainties exist due to non-thermodynamic contributions (O'Gorman and Schneider, 2009; O'Gorman, 2015).

The relationship between changes in IWV and precipitation (*P*) can be most easily examined by computing changes in atmospheric water vapour lifetime (*WVL*). The WVL then provides information on the extent to which this relationship is dependent on both the forcing mechanism and timescales of response, and the extent to which there is inter-model agreement on this relationship. The water vapour lifetime, or moisture residence time, is commonly expressed as the ratio between the time-averaged global-mean integrated water vapour and precipitation (Trenberth, 1998; Douville et al., 2002; Bosilovich et al., 2005; Schneider et al., 2010; Li et al., 2011; Kvalevåg et al., 2013). Studies identify a lifetime of 8-9 days for present-day conditions (van der Ent and Tuinenburg, 2017), although some argue for a substantially shorter lifetime of 4-5 days (Laderach and Sodemann, 2016). A historical increase in WVL is found from both models (Bosilovich et al., 2005; Kao et al., 2018) and observations (Li et al., 2011; Kao et al., 2018). The fact that water vapour content increases more rapidly than precipitation with rising surface temperatures implies an expected increase in the lifetime (Douville et al., 2002; Held and Soden, 2006; Schneider et al., 2010), and hence a slowing down of the hydrological cycle. However, global-mean precipitation or evaporation fluxes are commonly referred to as the strength of the hydrological cycle, which, in contrast, implies an intensification or acceleration of the hydrological cycle with global warming (e.g., Wu et al., 2013). Douville et al. (2002) note that this conclusion is somewhat misleading because it suggests faster turnover of water, which is not the case. Hence, when the global hydrological cycle is said to intensify or accelerate with warming, it should be made clear that this refers to the fluxes and not the cycle as a whole. Here we adopt the terminology from Douville et al. (2002), and use the

term amplification to indicate an increase in precipitation and evaporation rather than acceleration (which implies a decreased lifetime) of the hydrological cycle.

The WVL is a fundamental component of the hydrological cycle and is useful for studying how dynamical processes in the hydrological cycle are altered due to climate change (Laderach and Sodemann, 2016). For instance, potential increases in water vapour lifetime (expressed as $WVL=IWV/P$) imply that the moisture transport from the atmospheric boundary layer to the free troposphere must decrease, since the vertical moisture transport (M) is governed by $M=P/q$, where q is specific humidity in the boundary layer (Held and Soden, 2006), assuming that changes in q and IWV with temperature are proportional (some differences exist (O'Gorman and Muller, 2010)). A direct consequence of this is a weakening of the atmospheric circulation in the tropical Pacific, known as the Walker circulation, and this weakening is found both in observations and models (Vecchi et al., 2006). Stable water isotopes provide valuable knowledge on the evaporation and condensation history of atmospheric moisture, and more specifically on, e.g., proportions of convective and stratiform precipitation (Aggarwal et al., 2016) and past variability in high-latitude aerosol abundance (Markle et al., 2018). A positive correlation between WVL and stable isotope ratio in precipitation has been found from daily measurements at stations representing a range of climate regimes (Aggarwal et al., 2012), and better diagnostics of the impact of WVL on isotopes have been called for (Dee et al., 2018). It is suggested that the relationship between isotope ratio and the WVL could be used to improve the parameterizations of vertical mass-exchange in global climate models (GCMs) (Aggarwal et al., 2012), which is currently one of the major uncertainties in GCMs (Bony et al., 2015). Therefore, understanding the WVL has the potential to contribute to improved quantification of the hydrological cycle and its climate-induced changes.

A number of recent studies have looked at the impacts of different climate drivers on the fast and slow components of the hydrological cycle separately, but most of these studies have focused mainly on precipitation (Andrews et al., 2010; Bala et al., 2010; Ming et al., 2010; Kvalevåg et al., 2013; Xie et al., 2013; Samset et al., 2016; Myhre et al., 2018; Richardson et al., 2018b; Samset et al., 2018). In contrast to the slow (feedback) response, the fast response includes rapid adjustments to an external forcing and the initial radiative impact of the external forcing before changes in the global- and annual-mean surface temperature occur (Sherwood et al., 2015; Flaschner et al., 2016; Myhre et al., 2017). The common approach is to perform GCM simulations with prescribed sea surface temperatures (SST) to derive the fast response, and with coupled atmosphere-ocean to derive the total response. The slow response is the difference between the total and fast response. The slow response in global precipitation scales with the surface temperature change induced by each driver (Andrews et al., 2010; Samset et al., 2016), while the fast response scales with the change in the atmospheric component of the radiative forcing. Black carbon (BC) differs from most other climate drivers due to strong regional solar absorption in the atmosphere, and has been identified as a driver with large inter-model variability (Stjern et al., 2017).

In this study, we use GCM results from the Precipitation Driver Response Model Intercomparison Project (PDRMIP) (Myhre et al., 2017) to understand how the lifetime of water vapour has changed and is expected to change in the future according to GCM results in the Coupled Model Intercomparison Project phase 5 (CMIP5) (Taylor et al., 2011). PDRMIP

data are also used to explore how different climate drivers influence the distribution and magnitude of water vapour content throughout the atmosphere.

2 Methods

2.1 Precipitation Driver Response Model Intercomparison Project (PDRMIP)

Data from 11 GCMs involved in PDRMIP have been used – details about PDRMIP and the participating models (except ECHAM-HAM – see Supplementary Text S1) are given in Myhre et al. (2017). The core PDRMIP experiments consist of one base experiment, representing present-day conditions (pre-industrial for HadGEM2), and five perturbation experiments relative to base: doubling of the CO_2 concentration (hereafter denoted CO2x2), tripling of the CH_4 concentration (CH4x3), total solar irradiance increased by 2% (Sol+2%), five times increase in anthropogenic sulfate concentration or SO_2 emissions (SO4x5), and ten times increase in BC concentration or emissions (BCx10). Each experiment has been run with two model set-ups: with fixed SSTs, and with a coupled model configuration, being run for at least 15 and 100 years, respectively. Analyses are here based on years 6-15 from the fixed SST experiments and years 51-100 from the coupled experiments. Each model has run one ensemble member, but the model-mean water vapour lifetime sensitivity (WVLS; see Section 2.3) for each experiment differs by only 3% or less if results from years 51-75 or 76-100 are used instead of years 51-100 from the coupled experiments; this indicates a strong signal-to-noise ratio.

All model data have been regridded to T42 horizontal resolution, and, in the case of 3D data, to 60 vertical layers stretching from the surface to 0.1 hPa. In Fig. S1, IWV in the PDRMIP base experiment has been compared with observations from MODIS Aqua and Terra level 3 data (downloaded from https://giovanni.gsfc.nasa.gov/giovanni/), and the cycle 36 output from the European Centre for Medium Range Weather Forecasts Integrated Forecast System model for year 2010. Four of the PDRMIP models did not have 3D fields with specific humidity available, but for these models the specific humidity was calculated based on temperature, pressure and relative humidity in each grid box and for each month.

2.2 Coupled Model Intercomparison Project Phase 5 (CMIP5)

Data from 26 GCMs participating in CMIP5 (Taylor et al., 2011) were obtained (see Fig. 1 for model names) for the historical (1850-2005) and RCP8.5 (a “business-as-usual” pathway) (van Vuuren et al., 2011) (2006-2100) experiments, and for the variables surface air temperature, evaporation and water vapour path (here denoted integrated water vapour). The WVL was calculated by taking the global and 20-year mean IWV divided by evaporation (evaporation and precipitation are equal in the global mean).

Atmos. Chem. Phys. Discuss., https://doi.org/10.5194/acp-2019-121
Manuscript under review for journal Atmos. Chem. Phys.
Discussion started: 19 March 2019

2.3 Water vapour lifetime sensitivity

The global-mean water vapour lifetime sensitivity follows the approach of Kvalevåg et al. (2013) and is calculated as

$$WVL_i = \frac{IWV_i}{P_i}$$

$$\Delta WVL = WVL_i - WVL_{base}$$

$$WVLS = \frac{\Delta WVL}{\Delta T_s}$$

where WVL_i is the lifetime (in days), IWV_i is the global-mean integrated water vapour (kg m^{-2}), and P_i is the global-mean precipitation (kg m^{-2} day^{-1}) for a perturbation experiment *i*. The water vapour lifetime change, ΔWVL, is the difference between the lifetime in the perturbation and base experiments. The WVLS is the lifetime change divided by the global-mean surface temperature change, ΔT_s. The ΔWVL due to fast responses has been split into contributions from *IWV* and *P* by calculating the ΔWVL twice, with the *IWV* and *P* terms held constant one at a time.

3 Results and discussion

3.1 Water vapour lifetime and sensitivity

The CMIP5 pre-industrial multi-model mean value for the WVL is 7.8±0.5 days, and all models show an increase over both the historical and future time period (Fig. 1a) (a paired sample *t*-test shows that the multi-model mean increases are significant). A substantial increase of the lifetime from a present-day (i.e. 1986-2005) value of 8.2±0.5 to 9.9±0.7 days towards the end of the century is projected by the mean of CMIP5 models assuming RCP8.5, because increases in IWV are larger than for precipitation (Fig. 1b). Also, nearly 75% of the models show a stronger WVLS for the historical period than for the future, with model-mean values of 0.55±0.1 days/K and 0.47±0.06 days/K, respectively, and a paired sample *t*-test shows that the two values are significantly different. The present-day lifetime of 8.2±0.5 days from CMIP5 is close to, but slightly lower than, a recent assessment using reanalysis data of 8.9±0.4 days (van der Ent and Tuinenburg, 2017).

To further understand these differences, it is instructive to investigate WVLS for each of the fast and slow responses, and for each of the five climate drivers studied in PDRMIP. The response to surface temperature changes (i.e., slow response) dominates the change for all drivers except BCx10 (Fig. 2a), but the fast response is still a significant enhancement to the slow response for CO2x2 (27% of the total). For CH4x3, the fast response is 30% of the total, but with large differences between models (range of 8%-58%). All models (except HadGEM3) show that the fast response is more important than the slow response for BCx10, because BC is the driver with the strongest atmospheric temperature increase for the fast response. These results support earlier single-model findings (Kvalevåg et al., 2013). The slow response is remarkably similar between models and drivers, again with the exception of BCx10, which has an inter-model range of 0.10-0.45 days/K. Separating the fast response into contributions from changes in atmospheric water vapour and precipitation (keeping in mind that the lifetime is defined as global water vapour divided by precipitation) reveals that both terms are large for BCx10, but that

reduced precipitation dominates the fast WVL changes (Fig. 2b). Interestingly, reduced precipitation dominates the fast WVL changes for CO2x2 as well, while increased atmospheric water vapour dominates for Sol+2%. For SO4x5, the small fast WVL change is dominated by reduced water vapour (note that increased sulphate leads to cooling) except for one model (NCAR-CESM1-CAM5), which has a different sign because it has perturbed emissions rather than concentrations and it includes the influence of sulphate on BC through coating. This leads to a heating of the atmosphere, and this effect dominates the direct sulphate effect because fast responses for sulphate are small.

3.2 Historical lifetime changes explained

By combining the PDRMIP results for individual drivers with radiative forcing since pre-industrial time, we can reproduce the pre-industrial to present-day WVL increase of 0.34±0.08 days from CMIP5 models within the uncertainties (Fig. 3a). There is an almost equal contribution from the slow temperature response and the fast response to the total lifetime change.

The PDRMIP estimate of historical lifetime change due to the slow (temperature) response in Fig. 3a was derived by first taking the mean of the slow lifetime change across all PDRMIP drivers in Fig. 2a. This value of 0.31 days K^{-1} was then multiplied with the multi-model mean CMIP5 historical surface temperature change of 0.64 K (not shown). The PDRMIP fast response contribution in Fig. 3a is the sum of the individual terms in Fig. 3b. These terms have been derived by combining the present-day radiative forcing for separate climate drivers from Myhre et al. (2013) with the radiative forcing and fast WVL change from PDRMIP models using the following equation for each PDRMIP model

$$\Delta WVL_{fast,historical,j} = \Delta WVL_{fast,PDRMIP,j} \times \frac{RF_{historical,j}}{RF_{PDRMIP,j}}$$

where *RF* is the radiative forcing (in W m^{-2}) and *j* designates the climate driver and corresponding PDRMIP experiment, e.g., CO_2 and CO2x2, respectively (see Table S1 for details and multi-model mean values). The bars in Fig. 3b have further been split into contributions from changes in precipitation and water vapour using the numbers in Fig. 2b. All calculations were done for each PDRMIP model, and Fig. 3 shows the multi-model mean results.

Disentangling the fast response into contributions from the main historical climate drivers shows that increased CO_2 concentrations constitute around half (~0.1 days) of the net increase due to the fast response, with the reduced precipitation term being three times as large as the contribution from increased water vapour (Fig. 3b). For aerosols, a substantial lifetime increase due to BC is partly counteracted by scattering aerosols, which reduce the WVL. The impact of aerosols contributes to the stronger WVLS in the historical period compared to the future simulations in the CMIP5 models (Fig. 1b), since aerosol and aerosol precursor emissions are projected to decrease strongly towards the end of the century in the RCPs (Rogelj et al., 2014).

3.3 Zonal- and annual-mean changes in IWV

Figure 4 shows that the slow responses of global-mean water vapour per degree change in surface temperature differ between drivers, but are fairly close to the 7%/K that we expect from the Clausius-Clapeyron relation. However, these

differences are amplified by the fast response, which adds to the pure surface temperature related response, most notably for BCx10, which changes from 7.5±1%/K to 9.8±2%/K between the slow and total response.

Integrated water vapour increases much more than evaporation and precipitation at nearly all latitudes and for all five PDRMIP drivers (Fig. 4; Fig. S2-3). However, the total global-mean increase in IWV differs strongly between each driver, with BCx10 at 9.8±2%/K and SO4x5 at 6.4±0.9%/K. The estimated global IWV increase for BCx10 ranges from 6.8 to 13%/K for the different PDRMIP models, while locally decreasing in some regions (Fig. S4). BCx10, and to some extent SO4x5, show steep north-south gradients in the IWV change, emphasising the strong regional influences of these short-lived compounds (Fig. 4; Fig. S3-4). In contrast to the other climate drivers, precipitation decreases and water vapour increases strongly for BCx10, and this explains why the WVLS for BCx10 is more than twice as large as for any other driver (Fig. 2a).

3.4 Changes to global-mean vertical profiles

For the fast response from CO2x2, the change in the specific humidity profile differs considerably from what would be expected by the Clausius-Clapeyron relation when assuming that relative humidity stays constant (Fig. 5a; Fig. S5-6), a common assumption in climate change studies (Allen and Ingram, 2002). This indicates that the changes are not only temperature-driven. The specific humidity change for CO2x2 is around half of the expected temperature-induced change throughout most of the lower troposphere, explained by a tropospheric relative humidity decrease that peaks near 800 hPa (Fig. 5c). Over land, this lower than expected increase in specific humidity is particularly evident in the lower troposphere (Fig. S5), and this could be explained by the physiological effect since increased CO_2 leads to less evaporation from vegetation (Richardson et al., 2018a). CH4x3 shows some of the same tendency as CO2x2 (Fig. 5a) but without any considerable change in relative humidity (Fig. 5c), while Sol+2% largely follows the temperature-induced change in specific humidity (Fig. 5a). In contrast to the CO2x2 experiment, BCx10 mostly yields a small increase in relative humidity (Fig. 5c), especially close to the surface, and therefore the specific humidity change for BCx10 is larger than the temperature-induced change throughout most of the troposphere. It is also worth noting the different lapse rates, broadly with temperature changes decreasing with height for CO2x2 and increasing with height for BCx10 (Fig. 5d; Fig. S6), and this has implications for atmospheric stability.

Changes in specific humidity profiles for the slow response (Fig. 5b) show that the assumption of constant relative humidity does hold, and, when normalized with ΔT_s, they are similar between the drivers, with a small exception for SO4x5. Also, some differences can be seen for BCx10 with a discrepancy between the actual specific humidity change and the temperature-driven change between the surface and 800 hPa (Fig. 5b), and this is due to decreased relative humidity, especially over land (Fig. S7). Earlier studies have shown a strong land-ocean contrast in the response of near-surface relative humidity to global warming, mainly due to greater warming over land than ocean (Byrne and O'Gorman, 2016). Inspection of near-surface relative humidity changes shows that patterns of reduced relative humidity over land and increased over oceans are rather similar between drivers for the slow response (Fig. 6). However, the fast response constitutes a large part of the total response for all drivers. For CO2x2, fast responses amplify the land-ocean contrast

considerably, while for BCx10, fast responses lead to strong increases in relative humidity over large land regions, and these outweigh the reductions over land in the slow response.

4 Conclusions

Based on new model simulation data sets we can explain the historical increase in water vapour lifetime and quantify how this may change in the future. If emissions evolve according to a business-as-usual pathway, the WVL could increase by 25% by the end of the 21st century because of the large expected temperature changes, and despite the projected aerosol emission reductions leading to a lower water vapour lifetime sensitivity. The increased lifetime means that the hydrological cycle slows down considerably with global warming, but the cycle is still amplified because both precipitation and water vapour content increase globally.

Among the climate drivers studied here (CO_2, methane, solar irradiance, BC, and sulphate), WVL changes are most sensitive to perturbations in BC aerosols (1.1±0.4 days per Kelvin increase in T_s), due to strong increases in IWV with temperature combined with a precipitation reduction (contrary to precipitation increase for the other drivers). According to model calculations, an increase in WVL of 4-5% between pre-industrial and present-day has already occurred, and around half of this increase is due to fast atmospheric responses. Aerosol concentration changes, and BC in particular, strongly modify the fast WVL change and contribute to large inter-model uncertainty.

Due to known relations between precipitation, moisture and convective mass flux, an increase in WVL strongly indicates a subsequent reduction in global-mean vertical mass flux. Specifically, this involves a weakened tropical Pacific atmospheric circulation (Vecchi et al., 2006), but a further set of model integrations with the additional diagnostics would be required to firmly establish this. In addition, a longer WVL implies a higher heavy isotope ratio, due to the correlation between isotopes and WVL (Aggarwal et al., 2012), and this in turn indicates a larger fraction of convective vs. stratiform precipitation (Aggarwal et al., 2016).

Author contribution

GM and ØH designed the study. ØH performed the analysis and was the primary writer and received input from all authors, especially GM.

Acknowledgements

Ø.H., G.M., B.H.S. and K.A. were funded by the Research Council of Norway (RCN), through the grant NAPEX (229778). Supercomputer facilities were provided by NOTUR. Simulations with GISS-E2 used resources provided by the NASA High-End Computing Program through the NASA Center for Climate Simulation at Goddard Space Flight Center. M.K. and A.V.

were supported by the Natural Environment Research Council (NERC) under grant number NE/K500872/1. Simulations with HadGEM3-GA4 were performed using the MONSooN system, a collaborative facility supplied under the Joint Weather and Climate Research Programme, which is a strategic partnership between the Met Office and NERC. T. T. was supported by the supercomputer system of the National Institute for Environmental Studies, Japan, the Environment Research and Technology Development Fund (S-12-3) of the Ministry of the Environment, Japan and JSPS KAKENHI Grant Number JP15H01728 and JP15K12190. D.O. and A.K. were supported by RCN through the projects EarthClim (207711/E10), EVA (229771), the NOTUR (nn2345k) and NorStore (ns2345k) projects, and through the Nordic Centre of Excellence eSTICC (57001) and the EU H2020 project CRESCENDO (641816). T.B.R. was supported by NERC training award NE/K007483/1, and acknowledges use of the MONSooN system. Computing resources for J.F.L. (ark:/85065/d7wd3xhc) were provided by the Climate Simulation Laboratory at NCAR's Computational and Information Systems Laboratory, sponsored by the National Science Foundation and other agencies. Computing resources for the simulations with the MPI330 ESM model were provided by the German Climate Computing Center (DKRZ), Hamburg. Computing resources for O.B. were provided by GENCI at the TGCC under allocation gen2201. T.A. was supported by the Joint UK BEIS/Defra Met Office Hadley Centre Climate Programme (GA01101). P.S. acknowledges funding from the European Research Council project RECAP under the EU's H2020 research and innovation programme with grant agreement 724602 and the EU's FP7/2007-2013 projects BACCHUS under grant agreement 603445. D.W.P. acknowledges funding from NERC projects NE/L01355X/1 (CLARIFY) and NE/J022624/1 (GASSP). The ECHAM-HAM simulations were performed using the ARCHER UK National Supercomputing Service. We acknowledge the World Climate Research Programme's Working Group on Coupled Modelling, which is responsible for CMIP, and we thank the climate modeling groups for producing and making available their model output. For CMIP the U.S. Department of Energy's Program for Climate Model Diagnosis and Intercomparison provides coordinating support and led development of software infrastructure in partnership with the Global Organization for Earth System Science Portals. The PDRMIP model results are available at http://cicero.uio.no/en/PDRMIP. The CMIP5 data are available at http://pcmdi9.llnl.gov/. We thank Camilla Stjern for comments to the manuscript.

References

Aggarwal, P. K., Alduchov, O. A., Froehlich, K. O., Araguas-Araguas, L. J., Sturchio, N. C., and Kurita, N.: Stable isotopes in global precipitation: A unified interpretation based on atmospheric moisture residence time, Geophys. Res. Lett., 39, 6, 10.1029/2012gl051937, 2012.

Aggarwal, P. K., Romatschke, U., Araguas-Araguas, L., Belachew, D., Longstaffe, F. J., Berg, P., Schumacher, C., and Funk, A.: Proportions of convective and stratiform precipitation revealed in water isotope ratios, Nature Geoscience, 9, 8, 624-+, 10.1038/ngeo2739, 2016.

Allen, M. R., and Ingram, W. J.: Constraints on future changes in climate and the hydrologic cycle, Nature, 419, 6903, 224-232, 10.1038/nature01092, 2002.

Andrews, T., Forster, P. M., Boucher, O., Bellouin, N., and Jones, A.: Precipitation, radiative forcing and global temperature change, Geophys. Res. Lett., 37, L14701, 10.1029/2010gl043991, 2010.

Bala, G., Caldeira, K., and Nemani, R.: Fast versus slow response in climate change: implications for the global hydrological cycle, Clim. Dyn., 35, 2-3, 423-434, 10.1007/s00382-009-0583-y, 2010.

Bony, S., Stevens, B., Frierson, D. M. W., Jakob, C., Kageyama, M., Pincus, R., Shepherd, T. G., Sherwood, S. C., Siebesma, A. P., Sobel, A. H., Watanabe, M., and Webb, M. J.: Clouds, circulation and climate sensitivity, Nature Geoscience, 8, 4, 261-268, 10.1038/ngeo2398, 2015.

Bosilovich, M. G., Schubert, S. D., and Walker, G. K.: Global changes of the water cycle intensity, J. Clim., 18, 10, 1591-1608, 10.1175/jcli3357.1, 2005.

Boucher, O., Randall, D., Artaxo, P., Bretherton, C., Feingold, G., Forster, P., Kerminen, V.-M., Kondo, Y., Liao, H., Lohmann, U., Rasch, P., Satheesh, S. K., Sherwood, S., Stevens, B., and Zhang, X. Y.: Clouds and Aerosols, in: Climate Change 2013: The Physical Science Basis. Contribution of Working Group I to the Fifth Assessment Report of the Intergovernmental Panel on Climate Change, edited by: Stocker, T. F., Qin, D., Plattner, G.-K., Tignor, M., Allen, S. K., Boschung, J., Nauels, A., Xia, Y., Bex, V., and Midgley, P. M., Cambridge University Press, Cambridge, United Kingdom and New York, NY, USA, 571–658, 2013.

Byrne, M. P., and O'Gorman, P. A.: Understanding Decreases in Land Relative Humidity with Global Warming: Conceptual Model and GCM Simulations, J. Clim., 29, 24, 9045-9061, 10.1175/jcli-d-16-0351.1, 2016.

Chung, E. S., Soden, B., Sohn, B. J., and Shi, L.: Upper-tropospheric moistening in response to anthropogenic warming, Proc. Natl. Acad. Sci. U. S. A., 111, 32, 11636-11641, 10.1073/pnas.1409659111, 2014.

Dee, S. G., Nusbaumer, J., Bailey, A., Russell, J. M., Lee, J. E., Konecky, B., Buenning, N. H., and Noone, D. C.: Tracking the Strength of the Walker Circulation With Stable Isotopes in Water Vapor, J. Geophys. Res.-Atmos., 123, 14, 7254-7270, 10.1029/2017jd027915, 2018.

Douville, H., Chauvin, F., Planton, S., Royer, J. F., Salas-Melia, D., and Tyteca, S.: Sensitivity of the hydrological cycle to increasing amounts of greenhouse gases and aerosols, Clim. Dyn., 20, 1, 45-68, 10.1007/s00382-002-0259-3, 2002.

Flaschner, D., Mauritsen, T., and Stevens, B.: Understanding the Intermodel Spread in Global-Mean Hydrological Sensitivity, J. Clim., 29, 2, 801-817, 10.1175/jcli-d-15-0351.1, 2016.

Held, I. M., and Soden, B. J.: Robust responses of the hydrological cycle to global warming, J. Clim., 19, 21, 5686-5699, 10.1175/jcli3990.1, 2006.

Kao, A., Jiang, X., Li, L. M., Trammell, J. H., Zhang, G. J., Su, H., Jiang, J. H., and Yung, Y. L.: A Comparative Study of Atmospheric Moisture Recycling Rate between Observations and Models, J. Clim., 31, 6, 2389-2398, 10.1175/jcli-d-17-0421.1, 2018.

Kvalevåg, M. M., Samset, B. H., and Myhre, G.: Hydrological sensitivity to greenhouse gases and aerosols in a global climate model, Geophys. Res. Lett., 40, 7, 1432-1438, 10.1002/grl.50318, 2013.

Laderach, A., and Sodemann, H.: A revised picture of the atmospheric moisture residence time, Geophys. Res. Lett., 43, 2, 924-933, 10.1002/2015gl067449, 2016.

Li, L. M., Jiang, X., Chahine, M. T., Olsen, E. T., Fetzer, E. J., Chen, L. K., and Yung, Y. L.: The recycling rate of atmospheric moisture over the past two decades (1988-2009), Environmental Research Letters, 6, 3, 6, 10.1088/1748-9326/6/3/034018, 2011.

Markle, B. R., Steig, E. J., Roe, G. H., Winckler, G., and McConnell, J. R.: Concomitant variability in high-latitude aerosols, water isotopes and the hydrologic cycle, Nature Geoscience, 10.1038/s41561-018-0210-9, 2018.

Ming, Y., Ramaswamy, V., and Persad, G.: Two opposing effects of absorbing aerosols on global-mean precipitation, Geophys. Res. Lett., 37, L13701, 10.1029/2010gl042895, 2010.

Myhre, G., Shindell, D., Bréon, F.-M., Collins, W., Fuglestvedt, J., Huang, J., Koch, D., Lamarque, J.-F., Lee, D., Mendoza, B., Nakajima, T., Robock, A., Stephens, G., Takemura, T., and Zhang, H.: Anthropogenic and Natural Radiative Forcing, in: Climate Change 2013: The Physical Science Basis. Contribution of Working Group I to the Fifth Assessment Report of the Intergovernmental Panel on Climate Change, edited by: Stocker, T. F., Qin, D., Plattner, G.-K., Tignor, M., Allen, S. K., Boschung, J., Nauels, A., Xia, Y., Bex, V., and Midgley, P. M., Cambridge University Press, Cambridge, United Kingdom and New York, NY, USA, 659–740, 2013.

Myhre, G., Forster, P. M., Samset, B. H., Hodnebrog, O., Sillmann, J., Aalbergsjo, S. G., Andrews, T., Boucher, O., Faluvegi, G., Flaschner, D., Iversen, T., Kasoar, M., Kharin, V., Kirkevag, A., Lamarque, J. F., Olivie, D., Richardson, T. B., Shindell, D., Shine, K. P., Stjern, C. W., Takemura, T., Voulgarakis, A., and Zwiers, F.: PDRMIP A Precipitation Driver and Response Model Intercomparison Project-Protocol and Preliminary Results, Bull. Amer. Meteorol. Soc., 98, 6, 1185-1198, 10.1175/bams-d-16-0019.1, 2017.

Myhre, G., Kramer, R. J., Smith, C. J., Hodnebrog, Ø., Forster, P., Soden, B., Samset, B. H., Stjern, C. W., Andrews, T., Boucher, O., Faluvegi, G., Fläschner, D., Kasoar, M., Kirkevåg, A., Lamarque, J.-F., Olivié, D., Richardson, T., Shindell, D., Stier, P., Takemura, T., Voulgarakis, A., and Watson-Parris, D.: Quantifying the importance of rapid adjustments for global precipitation changes, Accepted in Geophysical Research Letters, doi:10.1029/2018GL079474, 2018.

O'Gorman, P. A., and Schneider, T.: The physical basis for increases in precipitation extremes in simulations of 21st-century climate change, Proc. Natl. Acad. Sci. U. S. A., 106, 35, 14773-14777, 10.1073/pnas.0907610106, 2009.

O'Gorman, P. A., and Muller, C. J.: How closely do changes in surface and column water vapor follow Clausius-Clapeyron scaling in climate change simulations?, Environmental Research Letters, 5, 2, 7, 10.1088/1748-9326/5/2/025207, 2010.

O'Gorman, P. A., Allan, R. P., Byrne, M. P., and Previdi, M.: Energetic Constraints on Precipitation Under Climate Change, Surv. Geophys., 33, 3-4, 585-608, 10.1007/s10712-011-9159-6, 2012.

O'Gorman, P. A.: Precipitation Extremes Under Climate Change, Current Climate Change Reports, 1, 2, 49-59, 10.1007/s40641-015-0009-3, 2015.

Richardson, T. B., Forster, P. M., Andrews, T., Boucher, O., Faluvegi, G., Flaschner, D., Kasoar, M., Kirkevag, A., Lamarque, J. F., Myhre, G., Olivie, D., Samset, B. H., Shawki, D., Shindell, D., Takemura, T., and Voulgarakis, A.: Carbon Dioxide Physiological Forcing Dominates Projected Eastern Amazonian Drying, Geophys. Res. Lett., 45, 6, 2815-2825, 10.1002/2017gl076520, 2018a.

Richardson, T. B., Forster, P. M., Andrews, T., Boucher, O., Faluvegi, G., Fläschner, D., Hodnebrog, Ø., Kasoar, M., Kirkevåg, A., Lamarque, J.-F., Myhre, G., Olivié, D., Samset, B. H., Shawki, D., Shindell, D., Takemura, T., and Voulgarakis, A.: Drivers of precipitation change: An energetic understanding, Accepted in Journal of Climate, 10.1175/jcli-d-17-0240.1, 2018b.

Rogelj, J., Rao, S., McCollum, D. L., Pachauri, S., Klimont, Z., Krey, V., and Riahi, K.: Air-pollution emission ranges consistent with the representative concentration pathways, Nature Clim. Change, 4, 6, 446-450, 10.1038/nclimate2178, 2014.

Samset, B. H., Myhre, G., Forster, P. M., Hodnebrog, O., Andrews, T., Faluvegi, G., Flaschner, D., Kasoar, M., Kharin, V., Kirkevag, A., Lamarque, J. F., Olivie, D., Richardson, T., Shindell, D., Shine, K. P., Takemura, T., and Voulgarakis, A.: Fast and slow precipitation responses to individual climate forcers: A PDRMIP multimodel study, Geophys. Res. Lett., 43, 6, 2782-2791, 10.1002/2016gl068064, 2016.

Samset, B. H., Myhre, G., Forster, P. M., Hodnebrog, Ø., Andrews, T., Boucher, O., Faluvegi, G., Fläschner, D., Kasoar, M., Kharin, V., Kirkevåg, A., Lamarque, J. F., Olivié, D., Richardson, T. B., Shindell, D., Takemura, T., and Voulgarakis, A.: Weak hydrological sensitivity to temperature change over land, independent of climate forcing, npj Climate and Atmospheric Science, 1, 1, 3, 10.1038/s41612-017-0005-5, 2018.

Santer, B. D., Mears, C., Wentz, F. J., Taylor, K. E., Gleckler, P. J., Wigley, T. M. L., Barnett, T. P., Boyle, J. S., Bruggemann, W., Gillett, N. P., Klein, S. A., Meehl, G. A., Nozawa, T., Pierce, D. W., Stott, P. A., Washington, W. M., and Wehner, M. F.: Identification of human-induced changes in atmospheric moisture content, Proc. Natl. Acad. Sci. U. S. A., 104, 39, 15248-15253, 10.1073/pnas.0702872104, 2007.

Schneider, T., O'Gorman, P. A., and Levine, X. J.: Water vapor and the dynamics of climate changes, Rev. Geophys., 48, 22, 10.1029/2009rg000302, 2010.

Sherwood, S. C., Bony, S., Boucher, O., Bretherton, C., Forster, P. M., Gregory, J. M., and Stevens, B.: Adjustments in the forcing-feedback framework for understanding climate change, Bull. Amer. Meteorol. Soc., 96, 2, 217-228, 10.1175/bams-d-13-00167.1, 2015.

Stjern, C. W., Samset, B. H., Myhre, G., Forster, P. M., Hodnebrog, O., Andrews, T., Boucher, O., Faluvegi, G., Iversen, T., Kasoar, M., Kharin, V., Kirkevag, A., Lamarque, J. F., Olivie, D., Richardson, T., Shawki, D., Shindell, D., Smith, C. J., Takemura, T., and Voulgarakis, A.: Rapid Adjustments Cause Weak Surface Temperature Response to Increased Black Carbon Concentrations, J. Geophys. Res.-Atmos., 122, 21, 11462-11481, 10.1002/2017jd027326, 2017.

Taylor, K. E., Stouffer, R. J., and Meehl, G. A.: An Overview of CMIP5 and the Experiment Design, Bull. Amer. Meteorol. Soc., 93, 4, 485-498, 10.1175/BAMS-D-11-00094.1, 2011.

Trenberth, K. E.: Atmospheric moisture residence times and cycling: Implications for rainfall rates and climate change, Climatic Change, 39, 4, 667-694, 10.1023/a:1005319109110, 1998.

Trenberth, K. E., Dai, A., Rasmussen, R. M., and Parsons, D. B.: The changing character of precipitation, Bull. Amer. Meteorol. Soc., 84, 9, 1205-1217, 10.1175/bams-84-9-1205, 2003.

van der Ent, R. J., and Tuinenburg, O. A.: The residence time of water in the atmosphere revisited, Hydrol. Earth Syst. Sci., 21, 2, 779-790, 10.5194/hess-21-779-2017, 2017.

van Vuuren, D. P., Edmonds, J., Kainuma, M., Riahi, K., Thomson, A., Hibbard, K., Hurtt, G. C., Kram, T., Krey, V., Lamarque, J. F., Masui, T., Meinshausen, M., Nakicenovic, N., Smith, S. J., and Rose, S. K.: The representative concentration pathways: an overview, Climatic Change, 109, 1-2, 5-31, 10.1007/s10584-011-0148-z, 2011.

Vecchi, G. A., Soden, B. J., Wittenberg, A. T., Held, I. M., Leetmaa, A., and Harrison, M. J.: Weakening of tropical Pacific atmospheric circulation due to anthropogenic forcing, Nature, 441, 7089, 73-76, 10.1038/nature04744, 2006.

Wentz, F. J., Ricciardulli, L., Hilburn, K., and Mears, C.: How much more rain will global warming bring?, Science, 317, 5835, 233-235, 10.1126/science.1140746, 2007.

Wu, P. L., Christidis, N., and Stott, P.: Anthropogenic impact on Earth's hydrological cycle, Nat. Clim. Chang., 3, 9, 807-810, 2013.

Xie, S. P., Lu, B., and Xiang, B. Q.: Similar spatial patterns of climate responses to aerosol and greenhouse gas changes, Nature Geoscience, 6, 10, 828-832, 10.1038/ngeo1931, 2013.

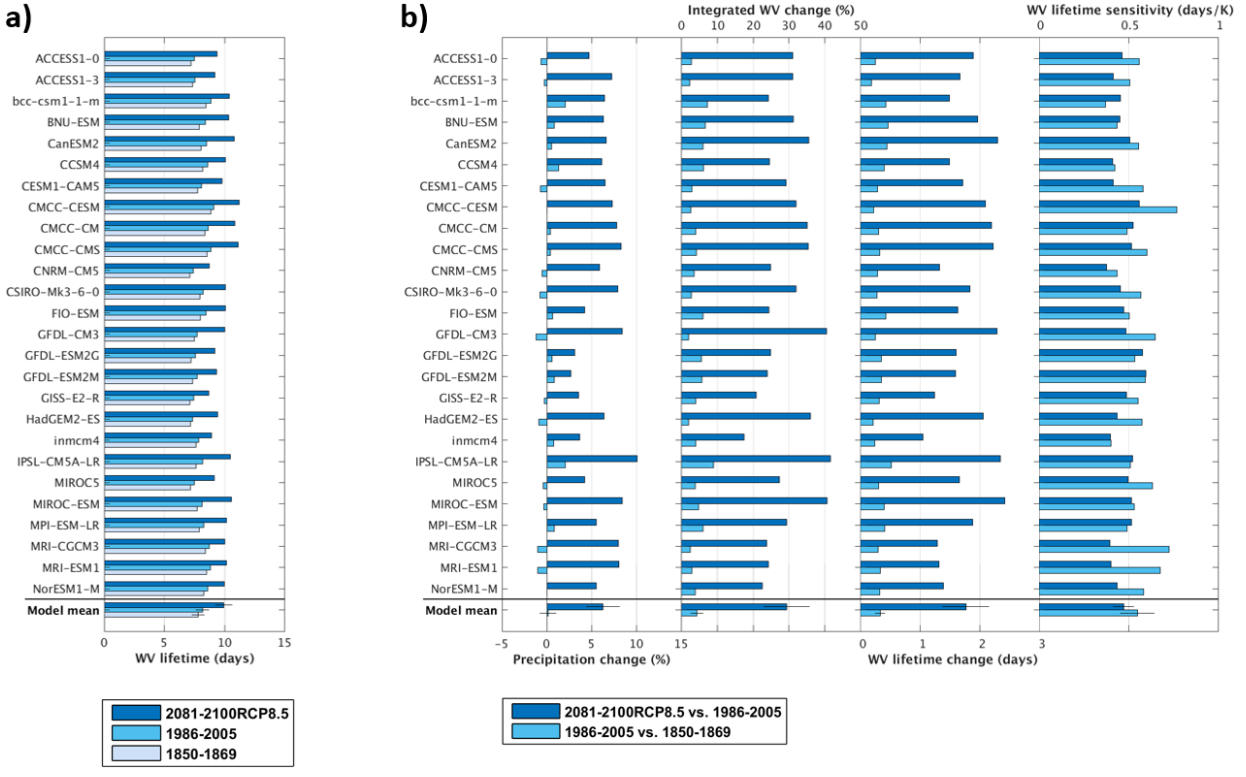

Figure 1: Historical and future water vapour lifetime in CMIP5 models. a) Water vapour (WV) lifetime (in days) for each of the three time periods, and b) changes in precipitation (%), integrated WV (%), WV lifetime (days), and WV lifetime sensitivity (WVLS; days/K) between each of the time periods. Error bars show the standard deviation representing the spread between the models. All values are global- and annual-means.

Atmos. Chem. Phys. Discuss., https://doi.org/10.5194/acp-2019-121
Manuscript under review for journal Atmos. Chem. Phys.
Discussion started: 19 March 2019

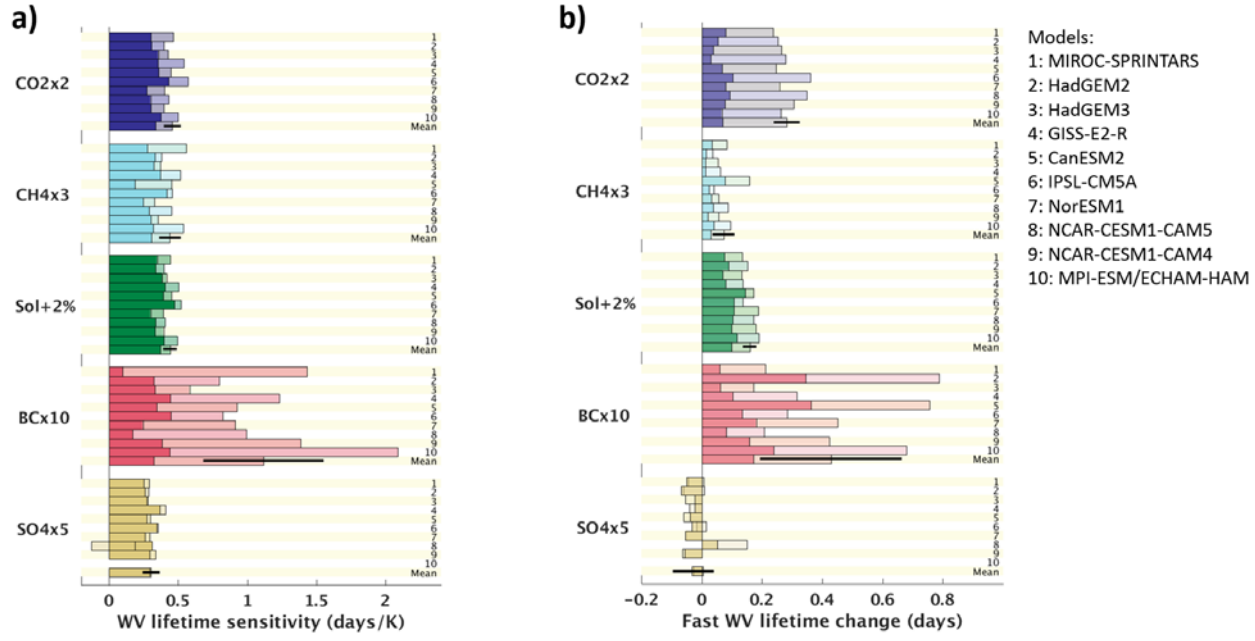

Figure 2: Water vapour lifetime changes for individual drivers. a) Water vapour (WV) lifetime sensitivity (in days/K) in PDRMIP models, split into slow (dark-coloured bars) and fast (light-coloured bars) responses for each driver. b) WV lifetime change (days) due to fast responses, split into contributions from changes in atmospheric water vapour (dark-coloured bars) and precipitation (light-coloured bars). The fast response in a) is not divided by ΔTs but calculated as the difference between the total and slow WV lifetime sensitivity (in days/K). In the few cases where the dark and light-coloured bars have opposite sign (e.g., SO4x5 model no. 8 in Fig. 2a), the vertical black line gives the net value. Error bars show the standard deviation representing the spread between the models.

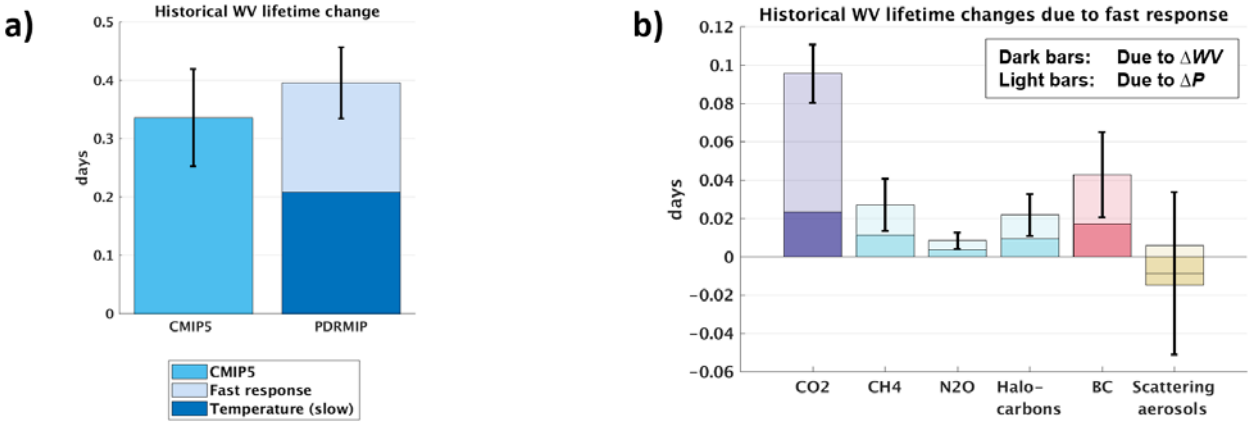

Figure 3: Contributions to historical water vapour lifetime change. a) Total historical change in water vapour (WV) lifetime from CMIP5 models compared to PDRMIP results with contributions from slow and fast responses. b) Historical WV lifetime change due to fast responses, split into different drivers and into contributions from changes in atmospheric integrated WV (dark-coloured bars) and precipitation (light-coloured bars). Error bars show the standard deviation representing the spread between the models.

Atmos. Chem. Phys. Discuss., https://doi.org/10.5194/acp-2019-121
Manuscript under review for journal Atmos. Chem. Phys.
Discussion started: 19 March 2019

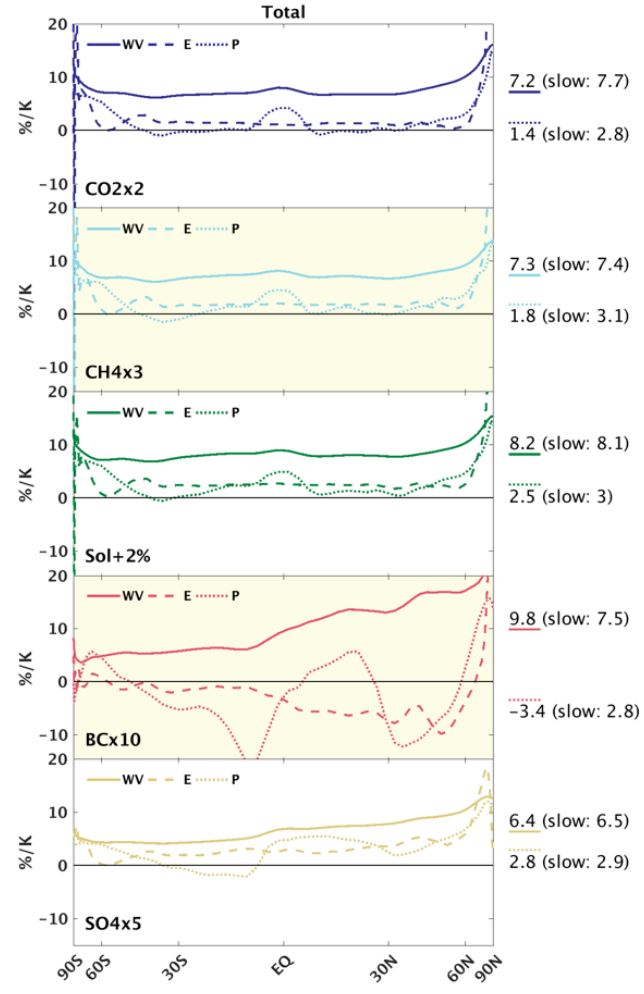

Figure 4: Zonal-mean relative changes (in %/K) in integrated water vapour (WV), evaporation (E), and precipitation (P) for five different drivers for the total response, divided by ΔT_s induced by each driver, using the mean of the PDRMIP results. Global-mean values are given to the right of each plot with the slow response given in parentheses (note that global-mean evaporation and precipitation are equal). In some cases, relative evaporation changes are large at very high latitudes and exceed the scale.

Atmos. Chem. Phys. Discuss., https://doi.org/10.5194/acp-2019-121
Manuscript under review for journal Atmos. Chem. Phys.
Discussion started: 19 March 2019

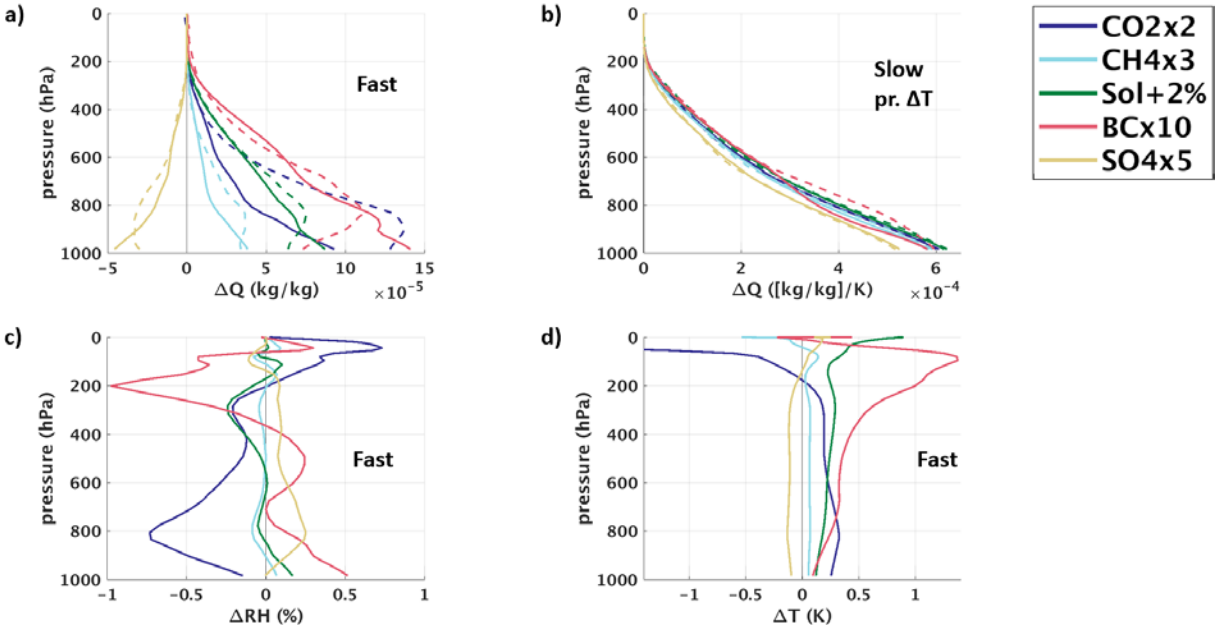

Figure 5: Vertical profile changes for individual drivers. a) Fast and b) slow changes in specific humidity (ΔQ), and fast changes in c) relative humidity (ΔRH) and d) temperature (ΔT), using the mean of the PDRMIP results. In a) and b), dashed lines show expected specific humidity changes from the Clausius-Clapeyron relation assuming constant relative humidity (calculated for each model, month and grid box, and with values at pressures <10 hPa set to zero because this approximation does not hold for low pressures). The slow response in b) is divided by ΔT_s induced by each driver.

Atmos. Chem. Phys. Discuss., https://doi.org/10.5194/acp-2019-121
Manuscript under review for journal Atmos. Chem. Phys.
Discussion started: 19 March 2019

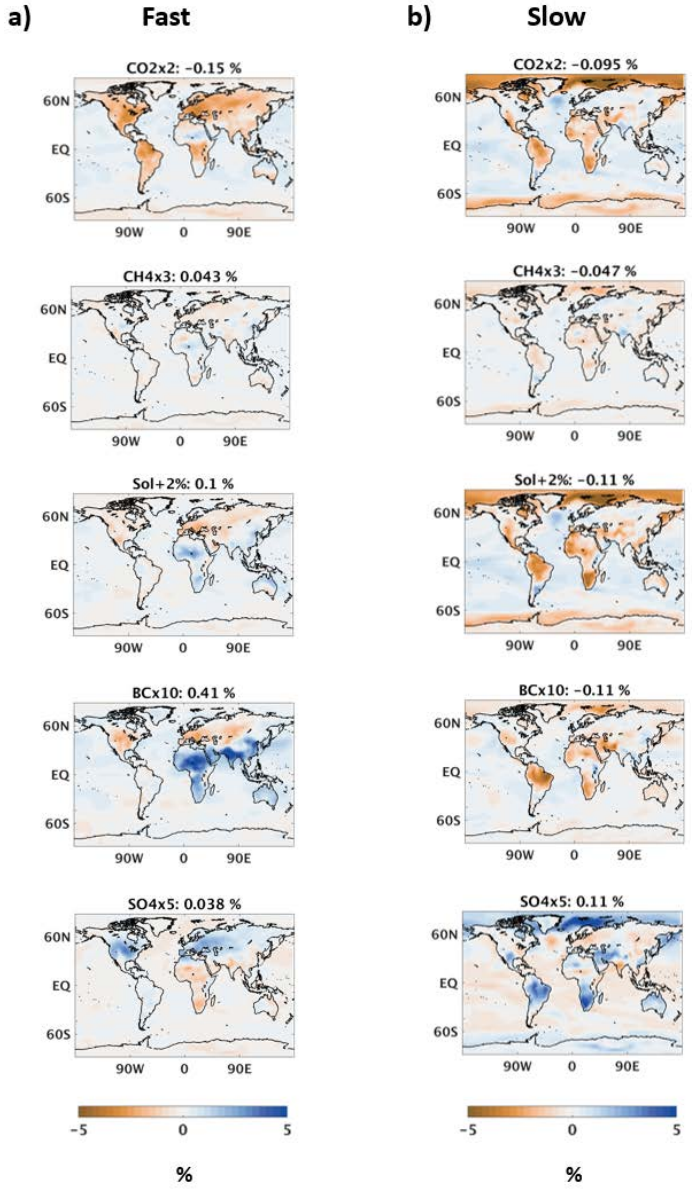

Figure 6: Maps of model mean absolute change in near-surface relative humidity (%) for each PDRMIP driver, separated into a) fast and b) slow responses. The plots are means of the six models with available data for near-surface relative humidity: CanESM2, HadGEM2, MIROC-SPRINTARS, NCAR-CESM1-CAM4, NCAR-CESM1-CAM5 and NorESM1.